ABSTRACT

Title of dissertation: Measuring topology of BECs in a synthetic dimensions lattice

Dina Genkina
Doctor of Philosophy, 2018

Dissertation directed by: Professor Ian Spielman
Department of Physics

Measuring topology of BECs in a synthetic dimensions lattice

by

Dina Genkina

Dissertation submitted to the Faculty of the Graduate School of the
University of Maryland, College Park in partial fulfillment
of the requirements for the degree of
Doctor of Philosophy
2018

Advisory Committee:
Professor Ian Spielman, Chair/Advisor

Table of Contents

List of Tables

List of Figures

Chapter 2: Introduction

2.1 Bose-Einstein condensation

2.1.1 Phase transition of a non-interacting Bose gas

Bose gases are characterized by the Bose-Einstein distribution giving the number of atoms $n(E_j)$ occupying each energy eigenstate E_j as

$$n(E_j) = \frac{1}{e^{(E_j-\mu)/k_\mathrm{B}T} - 1}, \tag{2.1}$$

where k_B is the Boltzmann constant, T is the temperature in Kelvin, μ is the chemical potential. Assuming the total atom number N is fixed, the chemical potential $\mu(T, N)$ ensures that the total occupation of all $\sum_j n(E_j) = N$.

The Bose distribution leads to Bose-Einstein condensation, the collapse of a macoscopic fraction of the atoms into the ground state. This comes as a direct consequence of the Bose distribution's characteristic -1 in the denominator. Consider the occupation number $n(E_j)$—it must remain positive, as a negative occupation number is unphysical. That means that the quantity $e^{(E_j-\mu)/k_\mathrm{B}T}$ must remain greater than 1, or $(E_j - \mu)/k_\mathrm{B}T < 0$ for all E_j. Therefore, $\mu \leq E_0$, where E_0 is the ground state energy.

Then, for a given temperature T, there is a maximum occupation number for each excited state given by $n(E_j) = \frac{1}{e^{E_j/k_\mathrm{B}T}-1}$. The only energy state whose occupation number is unbounded is the ground state, as $n(E_0)$ tends toward infinity as μ

tends towards 0. Therefore, as the temperature decreases, the maximum occupation of each excited state decreases until they can no longer support all of the atoms. The remaining atoms then have no choice but to collapse into the lowest energy level and Bose condense.

We will show this quantitatively for the case of a 3-D harmonically trapped gas of atoms, relavant to the experiments described in this thesis. It is convenient to define the fugacity $\zeta = e^{\mu/k_{\mathrm{B}}T}$, and re-write the Bose-Einstein distribution as eigenstate E_j as

$$n(E_j) = \frac{\zeta}{e^{E_j/k_{\mathrm{B}}T} - \zeta}. \tag{2.2}$$

The harmonic oscillator potentail can be written as

$$V(r) = \frac{1}{2}m(\omega_x^2 x^2 + \omega_y^2 y^2 + \omega_z^2 z^2), \tag{2.3}$$

where ω_x, ω_y and ω_z are the angular trapping frequencies along $\mathbf{e}_x$, $\mathbf{e}_y$, and $\mathbf{e}_z$. The eigenenergies with this potential are

$$E(j_x, j_y, j_z) = (\frac{1}{2} + j_x)\hbar\omega_x + (\frac{1}{2} + j_y)\hbar\omega_y + (\frac{1}{2} + j_z)\hbar\omega_z. \tag{2.4}$$

In order to find μ, we must find $\sum_{j_x,j_y,j_z} n(E(j_x, j_y, j_z))$ and set it equal to N. This task is greatly simplified by going to the continuum limit and finding the density of states. To do this, we neglect the zero-point energy (setting $E_0 = 0$, the effects of the zero-point energy are discussed in [3] section 2.5) and assume there is on average one state per volume element $\hbar^3\omega_x\omega_y\omega_z$. Then, the total number of states with energy less than or equal to some value ϵ is given by the volume of a prism made between points $(x, y, z) = (0, 0, 0), (\epsilon, 0, 0), (0, \epsilon, 0)$ and $(0, 0, \epsilon)$ in units of the volume element:

$$G(\epsilon) = \frac{\epsilon^3}{6\hbar^3\omega_x\omega_y\omega_z}. \tag{2.5}$$

The density of states is given by

$$g(\epsilon) = \frac{d}{d\epsilon}G(\epsilon) = \frac{\epsilon^2}{3\hbar^3\omega_x\omega_y\omega_z}. \tag{2.6}$$

Note that the occupation of the ground state is not included in this continuum picture. We can therefore use it only to calculate the total number of atoms in all of the excites states:

$$N_{\rm ex} = \int_0^\infty d\epsilon g(\epsilon)n(\epsilon) = \int_0^\infty d\epsilon \frac{\epsilon^2}{3\hbar\omega_x\omega_y\omega_z}\frac{\zeta}{e^{\epsilon/k_{\rm B}T}-\zeta} = \frac{(k_{\rm B}T)^3}{\hbar^3\omega_x\omega_y\omega_z}{\rm Li}_3(\zeta), \tag{2.7}$$

where ${\rm Li}_3(\zeta)$ is the polylogarithm function[1]. We define the mean trapping frequency $\bar{\omega} = (\omega_x\omega_y\omega_z)^{1/3}$ and the harmonic oscillator energy as $\hbar\bar{\omega}$, with the thermal energy in harmonic oscillator units $\tau = k_{\rm B}T/\hbar\bar{\omega}$, giving

$$N_{\rm ex} = \tau^3{\rm Li}_3(\zeta). \tag{2.8}$$

Finding the occupation number of the ground state from the Bose-Einstein distribution

$$N_0 = \frac{\zeta}{1-\zeta}, \tag{2.9}$$

we can then find the chemical potential, or equivalently the fugacity ζ, to satisfy

$$N = N_0 + N_{\rm ex}. \tag{2.10}$$

This is a transcendental equation that can only be solved numerically. We present an example of the solution in Figure 1. Here, we have calculated the fractional population in different harmonic oscillator energy levels for three different temperatures, using trapping frequencies are $\omega_x = \omega_y = \omega_z = 2\pi 50$ Hz, and atom number $N = 10^6$.

[1]This calculation was done with Wolfram Alpha, not Russian algebra skills

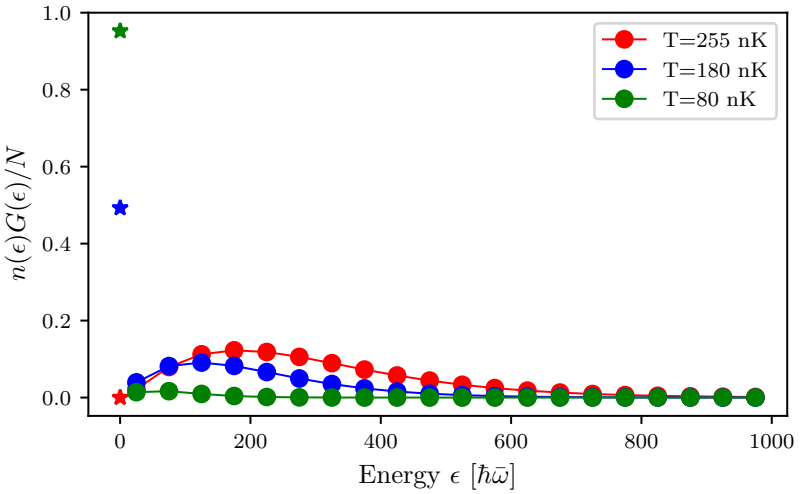

Figure 1: Occupation of energy states of a 3-D harmonic oscillator. The trapping frequencies are $\omega_x = \omega_y = \omega_z = 2\pi 50$ Hz, and the atom number is $N = 10^6$. Dots represent the total fractional population in 50 ajacent energy levels, including degeneracies. The stars represent the fractional population in just the ground state.

For enerigies above the ground state (dots in the figure), we binned 50 energy levels together, such that each dot represents the total fractional population in 50 adjacent levels. This was obtained by integrating eqn. 2.7 from $\epsilon - 25\hbar\bar{\omega}$ to $\epsilon + 25\hbar\bar{\omega}$. The stars represent the fractional population in just the ground state, calculated from eqn. 2.9. Note that at temperature $T = 255$ nK (red), the ground state population is consistent with a continuous extrapolation from the excited state populations and is almost zero. At lower temperatures, $T = 180$ nK (blue) the ground state population is in excess of any reasonable extrapolation from the excited state fractions, and at $T = 80$ nK (green) almost all the atoms are in the ground state.

The onset of Bose-Einstein condensation occurs at a critical temperature T_c. This temperature is defined as the temperature at which the occupation number of excited states is equal to the atom number, ie when the atoms have occupied all available excited states and any remaining atoms will have to pile into the ground state. Since the maximal occupation of the excited states will occur at $\mu = 0$,

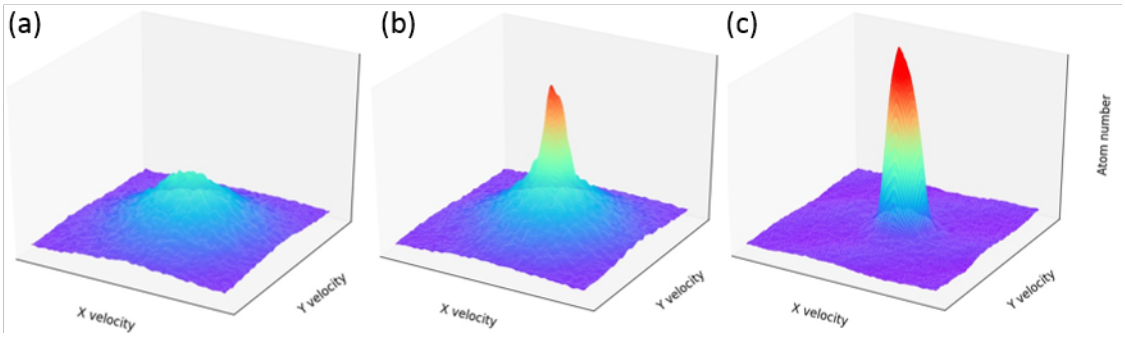

Figure 2: Time-of-flight images of atoms. (a) Above the critical temperature - the atoms are thermally distirbuted. (b) Below the critical temperature - about half of the atoms are condensed in the central peak. (c) Far below the critical temperature - almost all atoms are condensed in the central peak.

the occupation of the excited state is bounded from above by $N_{\mathrm{ex}}(\mu = 0)$, and the critical temperature is defined by

$$N = N_{\mathrm{ex}}(\mu = 0, T = T_c) = \frac{(k_{\mathrm{B}}T_c)^3}{\hbar^3\omega_x\omega_y\omega_z} Li_3(\zeta = 1). \tag{2.11}$$

Using $Li_3(1) \approx 1.202$, we obtain for a given atom number and trapping frequencies

$$T_c = \frac{1.202N}{k_{\mathrm{B}}^3}\hbar^3\omega_x\omega_y\omega_z. \tag{2.12}$$

For the parameters in Figure 1, $T_c = 225$ nK.

For temperatures below the critical temperature, the condensation fraction f_c—the fraction of atoms in the ground state—is directly related to the ratio of the temperature to the critical temperature:

$$f_c = 1 - \frac{N}{N_{\mathrm{ex}}} = 1 - \frac{(k_{\mathrm{B}}T)^3}{\hbar^3\omega_x\omega_y\omega_z} Li_3(\zeta = 1) = 1 - \left(\frac{T}{T_c}\right)^3, \tag{2.13}$$

where in the last step we have plugged in the definition of the critical temperature eqn. 2.12.

Figure 2 shows the progression towards condensation as the temperature of

a cloud of ^{87}Rb is decreased below T_c. The images are obtained via a time-of-flight measurement (see section **??**), where the atoms are allowed to expand freely, mapping the initial momentum to final position, imaged via absorption imaging (see section **??**). The x and y axes represent momentum along x and y, while the z axis represents the number of atoms. The z axis momentum is integrated over. Figure 2a shows a cloud above the condensation temperature - the momentum distribution is gaussian, given by the Maxwell-Boltzmann distribution. In fig. 2b, the temperature has been decreased below T_c, and about half the atoms have collapsed into the ground state, producing a large peak in atom number around zero momentum. In fig. 2c, the temperature has been decreased even further and almost all the atoms populate the central peak - the distribution is no longer gaussian but a sharp peak around zero momentum.

2.1.2 Interacting Bose gas

In the previous section, we assumed there was no interaction between the atoms other than that enforced by statistics. In this section, we will relax this assumption somewhat and describe the condensed atomic state through its characteristic Gross-Pitaevskii equation.

Since condensation occurs at very low temperatures, and thus very low kinetic energies, we can assume that any scattering processes between the atoms are s-wave and can be described simply by a scattering length a. For ^{87}Rb, relevant to experiments described in this thesis, the scattering length between two atoms in the $F = 2$ hyperfine state is $a = 95.44(7)a_0$ [4], where $a_0 = 5.29x10^{-11}$ m is the Bohr radius. The short-range interaction between two particles can be approximated as a contact interaction with an effective strength U_0 as (see [3] section 5.2.1):

$$U(r_1, r_2) = U_0\delta(r_1 - r_2) = \frac{4\pi\hbar^2 a}{m}\delta(r_1 - r_2), \tag{2.14}$$

where m is the atomic mass and δ is the Dirac delta function. The full Hamiltonian of the many-body system is then

$$H = \sum_i \frac{p_i}{2m} + V(r_i) + U_0 \sum_{i<j} \delta r_i - r_j, \tag{2.15}$$

where i labels the particles, p_i is the momentum, r_i is the position, and V is the external potential.

We make the mean field approximation by assuming that no interactions between two atoms take them out of the ground state, and hence all atoms can be assumed to be in the same single particle wavefunction, making the overall wavefunction

$$\Psi(r_1, r_2, ...r_N) = \prod_i^N \phi(r_i), \tag{2.16}$$

where ϕ is the single particle wavefunction. It is convenient to define the wavefunction of the condensed state, $\psi(r) = \sqrt{N}\phi(r)$, making the normalization $N = \int dr|\psi(r)|^2$.

The energy of this wavefunction under the Hamiltonian above is given by

$$E = \int dr \left[\frac{\hbar^2}{2m}|\nabla\psi(r)|^2 + V(r)|\psi(r)|^2 + \frac{1}{2}U_0|\psi(r)|^4\right] \tag{2.17}$$

Given N particles, there are $N(N-1)/2$ unique pairs of particles that can have a pairwise interaction, approximately equal to $N^2/2$ for large N. The N^2 is absorbed into the definition of ψ, but the factor of $1/2$ remains on the final interaction term. The task of finding the condensed eigenstate reduces to minimizing this energy under the normalization constraint $N = \int dr|\psi(r)|^2$. This can be done by using the method of Lagrange multipliers to minimize $E - \mu N$. Then, we can minimize this quantity by finding the point where the derivative with respect to ψ and ψ^* is zero.

Taking the derivative with respect to ψ^* we obtain

$$-\frac{\hbar^2}{2m}\nabla^2\psi(r) + V(r)\psi(r) + U_0|\psi(r)|^2\psi(r) = \mu\psi(r), \tag{2.18}$$

which is the Gross-Pitaevskii equation. This is a non-linear equation that generally needs to be solved numerically.

There is another approximation that can be made in cases where the atomic density is high enough that the interaction energy is significantly larger than the kinetic energy. Then, the kinetic term in the Hamiltonian can be neglected. This is called the Thomas-Fermi approximation. Then, the wavefunction is given simply by

$$|\psi(r)|^2 = \frac{\mu - V(r)}{U_0}. \tag{2.19}$$

In this approximation, the probability density simply takes the form of the inverse of the potential. In the case of a harmonically trapped BEC, it is shaped like an inverted parabola. The Thomas-Fermi radius, ie the extent of the particle wavefuntion, is the point where the probability density goes to zero: $\mu - V(r_0) = 0$. For a harmonic trap, along any direction, this is given by $r_0^2 = 2\mu/m\omega^2$.

Figure 3a shows an absorption image of a small fraction of a BEC in situ (see section **??**), meaning as they are in the trap - without expanding in time-of-flight. Therefore, the x and y axis represent position, while color represents the atom number. Figure 3b shows the atom number integrated over the y-axis in blue. The red dashed lines represent a best fit line to a Thomas-Fermi distribution, here an inverse parabola. The black dashed lines represent a best fit of a Gaussian to the atomic distribution. The Thomas-Fermi distirbution matches the atomic distribution more closely in the center where the density is high, but the Gaussian distribution does a better job at the tails of the distribution. This is due to the presence of some thermal atoms, which remain Maxwell-Boltzmann distributed.

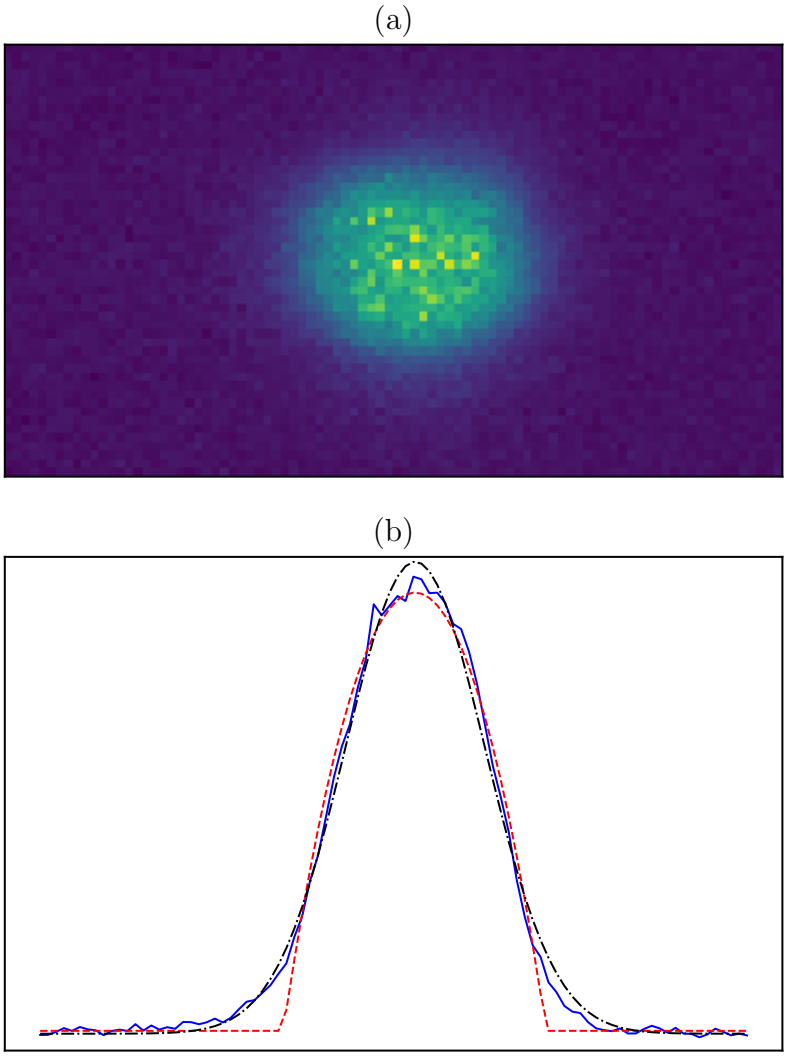

Figure 3: In situ measurement of a fraction of bose condensed atoms. (a) Absorption image taken of $\approx 1\%$ of the cloud. The x and y axes represent x and y position, while color represents the atom number. (b) The blue line repesents atom number as a function of position along hte x axis, integrated over the y axis. The black dashed line represents the best fit of a Gaussian function to the atomic distribution. The dashed red line represents the best fit of a Thomas-Fermi profile to the atomic distribution.

2.2 Degenerate Fermi Gas

2.2.1 Fermi statistcs and the onset of degeneracy

The occupation of different energy levels by Fermions is given by the Fermi-Dirac distribution:

$$n(\epsilon) = \frac{1}{e^{(\epsilon-\mu)/k_B T} + 1}. \tag{2.20}$$

The difference from the Bose-Einstein distribution is simply the sign of the 1 in the denominator. This has important implications, however. First, since e^x varies between 0 and inf, the occupation $n(\epsilon)$ varies between 1 and 0 - a consequence of the Pauli exclusion principle. Second, as the temperature T tends towards 0, there become two distinct cases: $\epsilon - \mu > 0$ and $\epsilon - \mu < 0$. If $\epsilon - \mu > 0$, $e^{(\epsilon-\mu)/k_B T}$ tends towards inf, and $n(\epsilon)$ tends towards 0. If $\epsilon - \mu < 0$, $e^{(\epsilon-\mu)/k_B T}$ tends towards 0, and $n(\epsilon)$ tends towards 1. Therefore, at $T = 0$, the energy states below the chemical potential μ are maximally occupied (with probability 1) and the energy states above the chemical potential are unoccupied.

We can use this to determine the chemical potential at $T = 0$ by constraining the total atom number:

$$N = \sum_j n(E_j) = \sum_{\epsilon_j < \mu} 1. \tag{2.21}$$

Again, we take the common example of the 3-D harmonic trap. Then the task reduces to simply finding the number of energy levels at or below a certain energy μ. This is given by eqn. 2.5. From this, we find the chemical potential at zero energy, which is known as the Fermi energy E_F, as

$$E_F = (6N)^{1/3} \hbar \bar{\omega}, \tag{2.22}$$

where $\bar{\omega} = (\omega_x \omega_y \omega_z)^{1/3}$ is the geometric mean of the three trapping frequencies.

From the Fermi energy, we can define the associated Fermi temperature T_F as

$$T_F = \frac{(6N)^{1/3}\hbar\bar{\omega}}{k_B}, \tag{2.23}$$

and the Fermi momentum $\hbar k_F$ as

$$\hbar k_F = \sqrt{2mE_F}, \tag{2.24}$$

where m is the mass of the Fermion.

For higher temeperatures, we can solve for the chemical potential, or the fugacity ζ, by integrating the Fermi-Dirac distribution weighted by the density of states (eqn. 2.6) to obtain

$$N = \int_0^\infty \frac{\epsilon^2}{2\hbar^3\bar{\omega}^3}\frac{\zeta}{e^{\epsilon/k_BT}+\zeta} = -\frac{(k_BT)^3}{\hbar^3\bar{\omega}^3}Li_3(-\zeta), \tag{2.25}$$

where Li_3 is again the polylogarithm function. Again, this is a transcendental equation that can be solved numerically. However, in contrast to the BEC case, we do not have to consider the ground state occupation separately, as it is bounded by 1 like every other state.

We show an example of the occupation distribution for different temperatures in Figure 4. Here, we have used the same parameter values as for the BEC case: $N = 10^6$ and $\omega_x = \omega_y = \omega_z = 2\pi 50$ Hz. The Fermi temperature for these parameters is $T_F = 436$ nK. For illustrative purposes, we plot $n(\epsilon)$, unweighted by the density of states $g(\epsilon)$. At zero temperature (red line in the figure), only states below the Fermi energy are occupied. At higher temperatures, the distribution is smoothed out (green and orange lines) until at the Fermi temperature there is almost no significance to the Fermi energy.

In contrast with Bose-Einstein condensation, the transition to a Degenerate

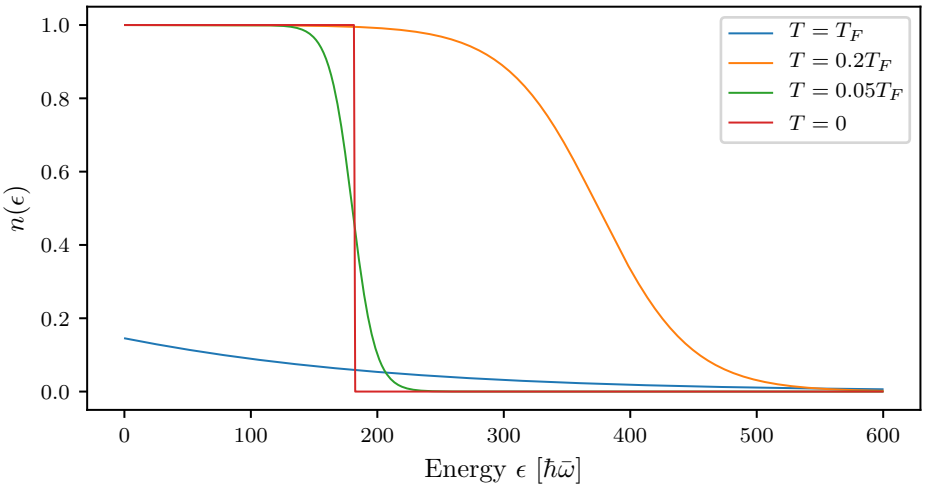

Figure 4: Occupation number as a function of energy for a Fermi gas of $N = 10^6$ atoms in a 3-D harmonic oscillator with frequencies $\omega_x = \omega_y = \omega_z = 2\pi 50$ Hz. The Fermi temperature for these parameters is $T_F = 436$ nK.

Fermi Gas (DFG) is not a phase transition, and there is no absolute measure of the onset of degeneracy. Instead, a Fermi gas can be considered degenerate when the occupation function $n(\epsilon)$ differs significantly from that of a thermal gas. This occurs when the temperature is of order $0.2T_F$.

2.2.2 Interactions and Feshbach resonances

Although the magnitgude of the contact interaction U_0 for DFGs is not intrinsially different from that of BECs. There are, however, two key differences. First, the Pauli exclusion principle forbids s-wave interactions between atoms of the same spin. Higher partial wave interactions are 'frozen out' at low temperatures, when the impact parameter of the collision becomes larger than the effective cross section of interactions (see [**?**], sec. 2.1.2). Therefore, in order to observe interactions, and indeed to cool the gas to degeneracy, another species needs to be present so that intraspecies s-wave interactions can occur. This can be a different atomic species or a different spin state of the same atom.

Second, the densities of standard DFGs ($\approx 10^{12}$ atoms/cm^3) are much lower than that of BECs ($\approx 10^{14}$ atoms/cm^3). Since the likelyhood of two-body collisions is proportional to the atomic density ρ^2, this leads to a much smaller effect of interactions in DFGs.

A widely used technique for enhancing interaction effects in DFGs is Feshbach resonances. A Feshbach resonance occurs between two spiecies (either atomic species or spin species of the same atom) when the open channel, ie the two particles independently in their external potential, energetically approaches a closed channel, ie a bound molecular state of the two species, shown schematically in Figure 5a.

Generally, the atoms in an open channel are energetically sensitive to a background magnetic field B via the hyperfine interaction $H_B = \mu \cdot B$, where μ is the magnetic dipole moment. Tuning the magnetic field should therefore tune the energy of the open channel. The molecular bound state may also have an overall magnetic moment, but it is generally not identical to that of the two atoms in the open channel, and therefore varies differently with the background field. Figure 5b shows an example where the bound state has zero magnetic moment. Here, the energy of both the closed and open channel as a function of backround magnetic field B is plotted in the vicinity of a Feshbach resonance. The resonance occures at a field B_0 where the energies of the two channels coincide.

Assuming there is at least infinitesmal coupling between the closed and open channels, as the energies of the two channels approach each other the perturbative correction term to the energy grows and the interaction between the atoms is effected. This is most easily seen in the s-wave case through changes the scattering length a. In the case where there are no inelastic two-body channels, such as for the ^{40}K resonance discussed in this thesis, the interatomic scattering length as a

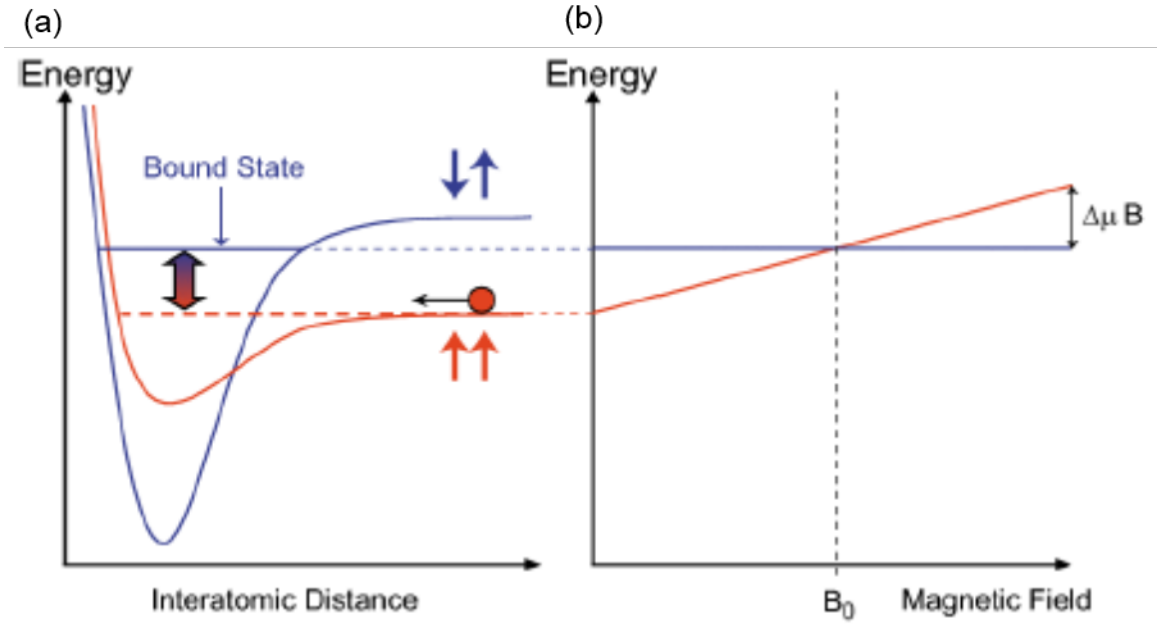

Figure 5: Schematic of a Feshbach resonance. (a) Pictoral representation of energy as a function of interatomic distance for an open channel (red) and closed channel (blue). (b) Energy as a function of background magnetic field B for the closed (blue) and open (red) channels. The energies coincide at the Feshbach resonance point B_0. Energy of Figure taken from [**?**].

function of background field is given by [?]

$$a(B) = a_{\mathrm{bg}} \left(1 - \frac{\Delta}{B - B_0}\right), \tag{2.26}$$

where a_{bg} is the background scattering length, Δ is the width of the resonance, and B_0 is the field value at which the resonance occurs. The scattering length diverges at the resonance.

The tunability of interactions provided by Feshbach resonances has allowed for creation of molecular Bose-Einstein condensates from Fermi gases [?, ?, ?] as well as observation of the phase transition from the Bardeen-Cooper-Schrieffer (BCS) superconduting regime to the BEC regime at sufficiently low temperatures [?, ?, ?, ?].

2.3 RbK apparatus

The rubidium-potassium (RbK) appartus at NIST Gaithersburg has been previously detailed in [?, ?, 8]. In this thesis, we will give a brief overview of the apparatus and how it is used to produce BECs of ^{87}Rb and DFGs of ^{40}K, and only give detailed documentation for those parts of the apparatus that differ from previous works.

A photograph of the main experiment is shown in Figure 6. This is mounted on an optical table, with the science chamber elevated above the surface of the table. The atoms start at the ovens (off to the right, not in the photograph) and travel down the Zeeman slower until they are trapped in the science chamber. The optical dipole trap laser, as well as the 1-D optical lattice laser, are located on the optical table and coupled into optical fibers, which are output on the main floor of breadboard before being sent towards the atoms. All other lasers are located on other optical table and brought over to the experiment table via optical fibers.

Figure 7 details the beam paths of the light going through the atoms. Figure

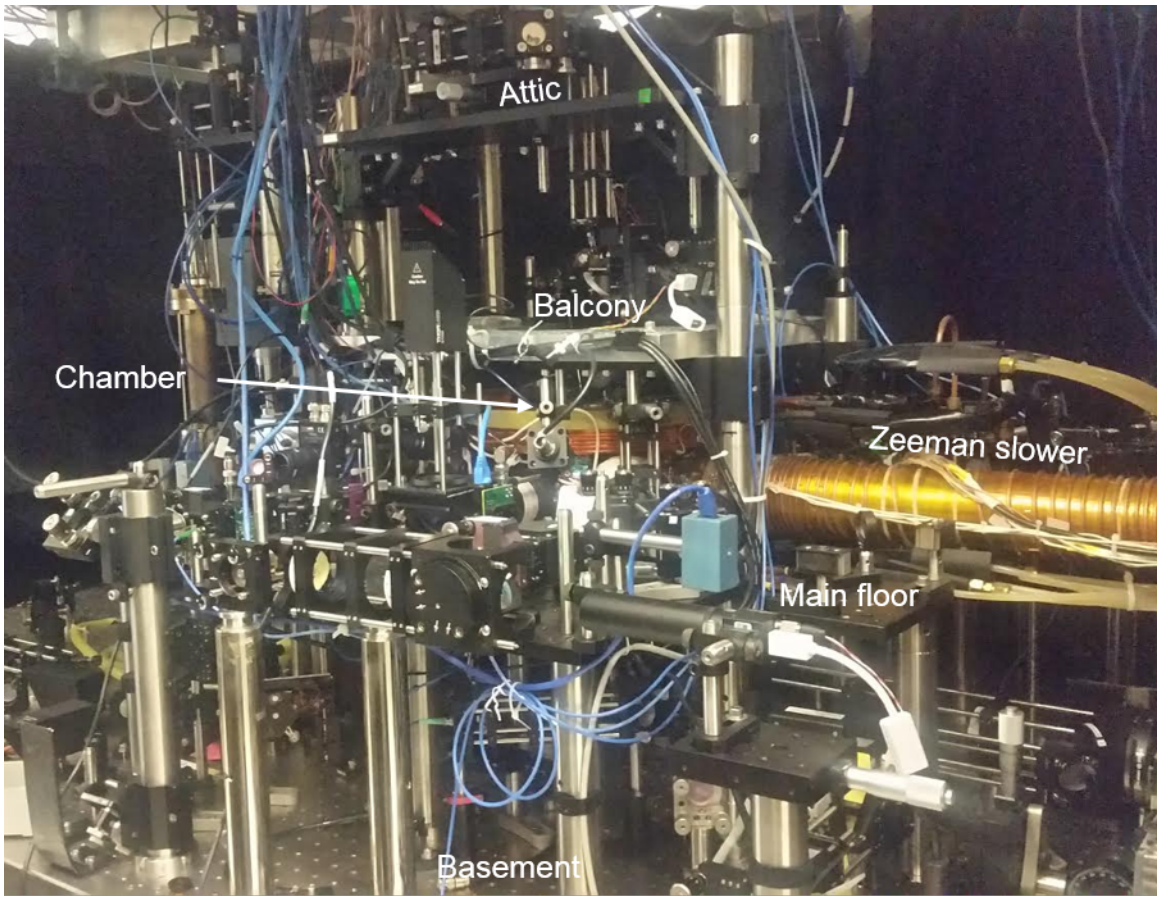

Figure 6: Photograph of RbK apparatus at NIST Gaithersburg. The main science chamber is at the center, hidden behind optics and coils. The Zeeman slower connects the atomic ovens (not shown) to the chamber. There are several levels of breadboards on which optics are mounted, labelled here as basement (surface of optical table), main floor, balcony and attic.

7a shows a side view of the apparatus. The up and down going MOTcooling beams are shown in red, reaching the atoms when the flipper mirrors M_{top} and M_{bottom} are flipped in. The down going probe beam, used for imaging along the $x-y$ axis both in situ and in time-of-flight, is shown in solid blue. The probe beam is split via a polarizing beam splitter cube to allow for both in situ and time-of-flight imagnig of the same cloud, shown in the inset in fig. 7b and described in greater detail in sec. 2.3.2. The dashed blue line represents the upward going probe beam introduced for alignment purposes, described in greater detail in sec. 2.3.2.

Figure 7b show's a bird's eye view of the apparatus, with optics on the main floor breadboard. The slower cooling (solid dark blue) and slower repump (dashed dark blue) are coming in from the left to slow the atoms as they are moving through the Zeeman slower. The remaining four MOT cooling beams, coming from four opposing directions, are shown in red. They reach the atoms when their flipper mirrrors, $M1-4$, are flipped in. All six flipper mirrors are computer controlled by the same digital channel, so they can be flipped in and out together. Only the beams going in through mirrors $M1$ and $M2$ are accompanied by MOT repump light, dashed red lines. The optical dipole trap beams (solid green) come from the same 1064 nm laser, and are split via an acousto-optic modulator into two orders, which enter from opposite directions and intersect each other at approximately a 90 degree angle, providing confinement along all three axes. There are three available Raman beams (solid magenta): Raman A, entering past the flipped-out $M2$ mirror, Raman B, at 90 degrees to Raman A entering past the $M1$ mirror, and Raman C, counter-propagating with Raman A and entering past the $M4$ mirror. There is a 1-D optical lattice beam (dashed green), also 1064 nm, sent in past the $M2$ mirror and retroreflected on the opposite end of the chamber to form a standing wave patter. Lastly, there is another imaging beam, imaging the atoms along the $x-z$ plane, going to a Flea3 camera.

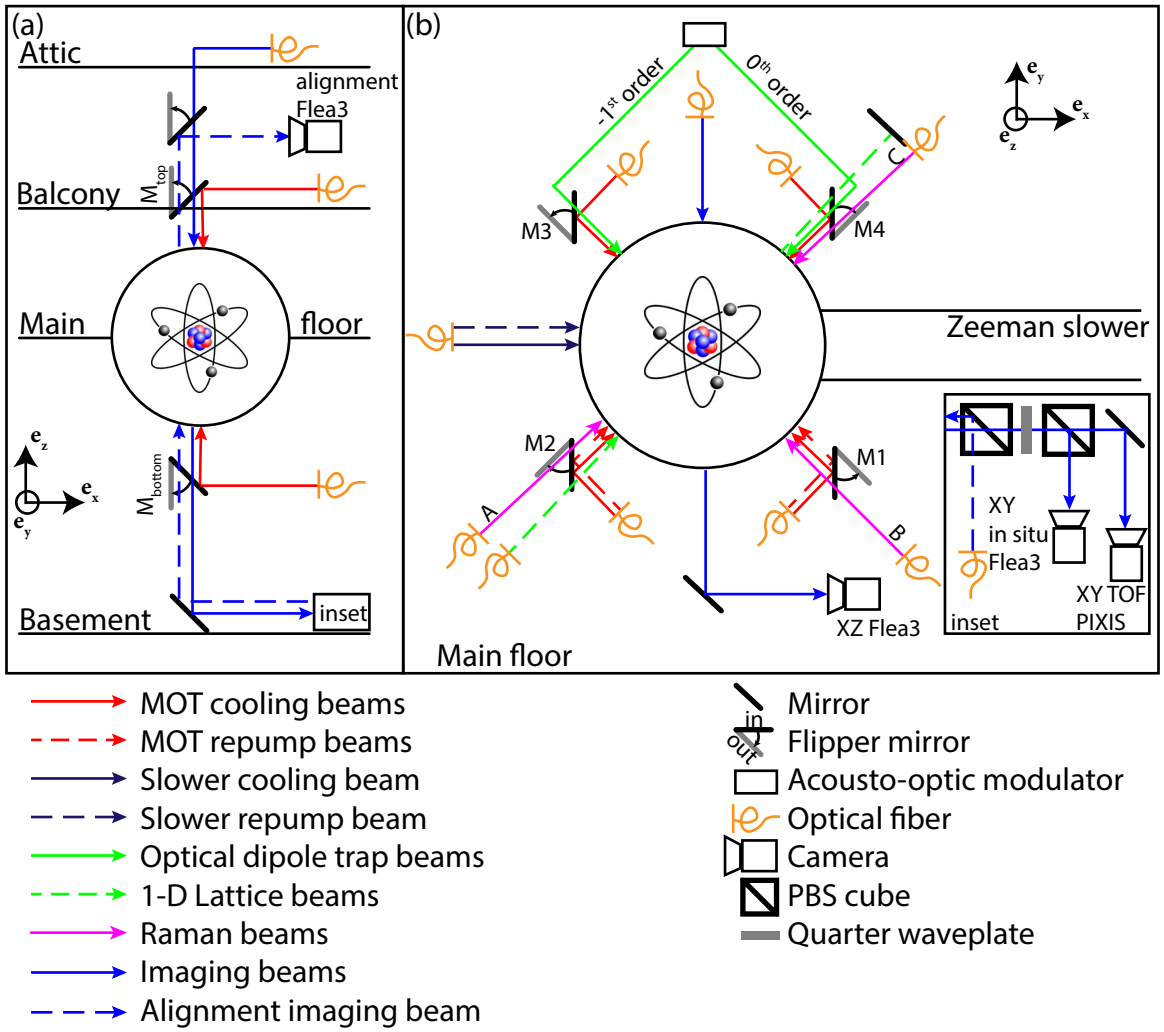

Figure 7: Schematic of RbK apparatus. (a) Side view of apparatus. Only beams propagating along the $e_{\mathbf{z}}$ direction through the atoms is pictured. (b) Top view of apparatus. Only beams propagating along the $x-y$ plane are shown. Schematic is not to scale and the angles are approximate

2.3.1 Procedure for making a BEC

Brief description of BEC making procedure

2.3.2 Changes to apparatus for Rubidium

Differences from Lauren's thesis:

Put master laser setup in PBS cube on XY imaging system Describe Hsin-I's new imaging path Describe extra lens for beam shaping the dipole trap

2.3.3 Procedure for making a DFG

Brief description of DFG making procedure (of old)

2.3.4 Current status of Potassium apparatus

Differences from Lauren's thesis: Describe 2D MOT'

Bibliography

[1] Daniel Adam Steck. Rubidium 87 d line data. Available online, http://steck.us/alkalidata, April 2018. revision 2.1.5.

[2] K. Jiménez-García, L. J. LeBlanc, R. A. Williams, M. C. Beeler, A. R. Perry, and I. B. Spielman. Peierls substitution in an engineered lattice potential. *Phys. Rev. Lett.*, 108:225303, May 2012.

[3] C.J. Pethick and H. Smith. *Bose-Einstein Condensation of Dilute Gases*. Cambridge University Press, Cambridge, UK, 2002.

[4] M. Egorov, B. Opanchuk, P. Drummond, B. V. Hall, P. Hannaford, and A. I. Sidorov. Measurement of s-wave scattering lengths in a two-component bose-einstein condensate. *Phys. Rev. A*, 87:053614, May 2013.

[5] H.J. Metcalf and P. van der Straten. *Laser Cooling and Trapping*. Graduate Texts in Contemporary Physics. Springer New York, 1999.

[6] N.W. Ashcroft and N.D. Mermin. *Solid State Physics*. Saunders College, Philadelphia, 1976.

[7] Nicola Marzari, Arash A. Mostofi, Jonathan R. Yates, Ivo Souza, and David Vanderbilt. Maximally localized wannier functions: Theory and applications. *Rev. Mod. Phys.*, 84:1419–1475, Oct 2012.

[8] Karina Jimenez-Garcia. *Artificial Gauge Fields for Ultracold Neutral Atoms*. PhD thesis, Joint Quantum Institute, National Institute of Standards and Technology, and the University of Maryland, 2012.

[9] Daniel Adam Steck. Quantum and atom optics. Available online at http://steck.us/teaching, January 2015. revision 0.12.2.

[10] Lindsey J. LeBlanc. *Exploring many-body physics with ultracold atoms*. PhD thesis, University of Toronto, 2011.

[11] K. v. Klitzing, G. Dorda, and M. Pepper. New method for high-accuracy determination of the fine-structure constant based on quantized hall resistance. *Phys. Rev. Lett.*, 45:494–497, Aug 1980.

[12] D. J. Thouless, M. Kohmoto, M. P. Nightingale, and M. den Nijs. Quantized hall conductance in a two-dimensional periodic potential. *Phys. Rev. Lett.*, 49:405–408, Aug 1982.

[13] Douglas R. Hofstadter. Energy levels and wave functions of bloch electrons in rational and irrational magnetic fields. *Phys. Rev. B*, 14:2239–2249, Sep 1976.

[14] M. C. Geisler, J. H. Smet, V. Umansky, K. von Klitzing, B. Naundorf, R. Ketzmerick, and H. Schweizer. Detection of a landau band-coupling-induced rearrangement of the hofstadter butterfly. *Phys. Rev. Lett.*, 92:256801, Jun 2004.

[15] B. Hunt, J. D. Sanchez-Yamagishi, A. F. Young, M. Yankowitz, B. J. LeRoy, K. Watanabe, T. Taniguchi, P. Moon, M. Koshino, P. Jarillo-Herrero, and R. C.

Ashoori. Massive Dirac Fermions and Hofstadter Butterfly in a van der Waals Heterostructure. *Science*, 340:1427, 2013.

[16] P. Zoller D. Jaksch. Creation of effective magnetic fields in optical lattices: the hofstadter butterfly for cold neutral atoms. *New Journal of Physics*, 5(1):56, 2003.

[17] M. Aidelsburger, M. Atala, M. Lohse, J. T. Barreiro, B. Paredes, and I. Bloch. Realization of the hofstadter hamiltonian with ultracold atoms in optical lattices. *Phys. Rev. Lett.*, 111(18):185301–, October 2013.

[18] Hirokazu Miyake, Georgios A. Siviloglou, Colin J. Kennedy, William Cody Burton, and Wolfgang Ketterle. Realizing the harper hamiltonian with laser-assisted tunneling in optical lattices. *Phys. Rev. Lett.*, 111:185302, Oct 2013.

[19] Gregor Jotzu, Michael Messer, Remi Desbuquois, Martin Lebrat, Thomas Uehlinger, Daniel Greif, and Tilman Esslinger. Experimental realization of the topological haldane model with ultracold fermions. *Nature*, 515(7526):237–240, Nov 2014.

[20] M Aidelsburger, M Lohse, C Schweizer, M Atala, J T Barreiro, S Nascimbène, N. R. Cooper, I. Bloch, and N. Goldman. Measuring the Chern number of Hofstadter bands with ultracold bosonic atoms. *Nature Physics*, 11(2):162–166, December 2014.

[21] M. Mancini, G. Pagano, G. Cappellini, L. Livi, M. Rider, J. Catani, C. Sias, P. Zoller, M. Inguscio, M. Dalmonte, and L. Fallani. Observation of chiral edge states with neutral fermions in synthetic hall ribbons. *Science*, 349(6255):1510–, Sep 2015.

[22] M Hafezi, S Mittal, J Fan, A Migdall, and J M Taylor. Imaging topological edge states in silicon photonics. *Nat. Photon.*, 7(12):1001–1005, October 2013.

[23] A. Celi, P. Massignan, J. Ruseckas, N. Goldman, I.B. Spielman, G. Juzeliunas, and M. Lewenstein. Synthetic gauge fields in synthetic dimensions. *Phys. Rev. Lett.*, 112(4):043001–, Jan 2014.

[24] B. K. Stuhl, H.-I. Lu, L. M. Aycock, D. Genkina, and I. B. Spielman. Visualizing edge states with an atomic bose gas in the quantum hall regime. *Science*, 349(6255):1514–, Sep 2015.

[25] Y. Aharonov and D. Bohm. Significance of electromagnetic potentials in quantum theory. *Phys. Rev.*, 115:485, 1959.

[26] Yakir Aharonov and Ady Stern. Origin of the geometric forces accompanying berry's geometric potentials. *Phys. Rev. Lett.*, 69(25):3593–3597, 1992.

[27] Dario Hügel and Belén Paredes. Chiral ladders and the edges of quantum Hall insulators. *Phys. Rev. A*, 89(2):023619, 2014.